ACADEMIA ROMÂNĂ
Revue Roumaine de Chimie
https://www.icf.ro/rrch/

Rev. Roum. Chim.,
2024, *69*(1–2), 63–74
DOI: 10.33224/rrch.2024.69.1-2.08

NEW MONOQUATERNARY SALTS OF *N*-HETEROCYCLES: SYNTHESIS AND ANTITUMOR ASSESSMENT**

Monica-Cornelia SARDARU,[a,b] Cristina-Maria AL MATARNEH,[a,b,*] Natalia SIMIONESCU,[a] Ionel I. MANGALAGIU,[b] Mariana PINTEALA[a] and Ramona DANAC[b,*]

[a]Center of Advanced Research in Bionanoconjugates and Biopolymers**,** "Petru Poni" Institute of Macromolecular Chemistry of Roumanian Academy, 41A Grigore Ghica Voda Alley, Iași 700487, Roumania
[b]Faculty of Chemistry, "Al. I. Cuza" University of Iași, 11 Carol I, Iași 700506, Roumania

Received August 30, 2023

This manuscript presents the synthesis, structural characterization, and antitumor evaluation of new monoquaternary salts derived from various *N*-heterocycles. For quinoline and quinoxaline, respectively, unexpected H-bonded mixtures of the reactants have been obtained. To assess their potential antitumor activity, the comprehensive panel of NCI's 60 human cancer cell lines was employed. Remarkably, mixtures **3g** and **3h** displayed significant inhibitory activity against leukemia, melanoma, and colon cancer cell lines. Furthermore, mixtures **3g** and **3h** displayed good cytotoxicity on MCF7 breast cancer cells, but not on normal fibroblasts, at 2.5×10^{-5} M, showing promise for therapeutic applications.

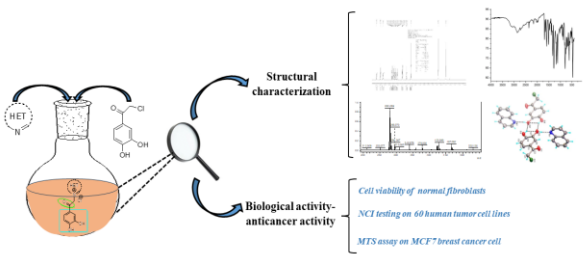

INTRODUCTION

In the realm of drug design, nitrogenous molecules hold a prominent position due to their numerous advantages over non-nitrogenous counterparts. The incorporation of nitrogen into a molecule enhances its basicity, resulting in a significant enhancement of its reactivity and interactions with other molecules. Furthermore, nitrogen atoms possess an exceptional capacity to establish strong hydrogen bonds with certain molecules, resulting in a heightened affinity for binding. One other noteworthy characteristic of nitrogenous compounds is their polarity. This property can be harnessed to fine-tune characteristics such as lipophilicity, water

* Corresponding authors: almatarneh.cristina@icmpp.ro or rdanac@uaic.ro
** Supplementary Information on https://www.icf.ro/rrch/ or https://revroum.lew.ro

solubility, and oral absorption, thus optimizing their pharmacological properties.[1]

Among the diverse array of nitrogenous heterocycles, the quinoline pattern stands out as a key component in natural alkaloids with various biological functions.[2] The quinoline ring system is the foundation for effective malaria therapies, such as quinine, chloroquine, mefloquine, and amodiaquine. Furthermore, quinoline analogs have demonstrated promise in combating cancer through multiple pathways,[1] including tyrosine kinase inhibition, alkylating agent activity, and tubulin inhibition.[3]

One quaternary isoquinoline alkaloid, berberine, exhibits considerable therapeutic potential against cancer. However, its limited absorption necessitates higher doses to achieve therapeutic objectives. Extensive research has focused on modifying the positive isoquinoline unit of berberine by grafting lengthy aliphatic chains or heterocycles to enhance its biological activity.[4]

Recently, considerable attention has been directed towards 6*H*-indolo[2,3-*b*]quinoxaline, owing to its remarkable pharmacological properties.[5] Acting on ATP binding cassette transporters, this compound displays antiviral activity against various viruses, cytotoxic effects, and the ability to modulate multidrug resistance. As an aza-analogue of the cytotoxic drugs cryptolepine and ellipticine, 6*H*-indolo[2,3-*b*]quinoxaline's planar structure facilitates DNA intercalation, leading to its diverse biological actions.[6]

Phthalazine derivatives have received significant interest due to their potent luminescence and photochromic properties, as well as their potential as drug candidates.[7] Some derivatives have demonstrated antimicrobial, antifungal, or anticancer effects, and others act as inhibitors of JAK, HER-2 tyrosine kinase, IRAK4, or MEK.[8]

The last century witnessed extensive pharmacological research on pyrrolopyridines, thanks to their unique structural elements, pyrrole, and pyridine. Pyrrole derivatives have exhibited a wide range of pharmacological activities and have been integrated into numerous medications targeting conditions such as inflammation, insomnia, migraines, Parkinson's disease, and erectile dysfunction.[9] Recently, fostemsavir received approval for the treatment of HIV. Pyrrolopyridine scaffolds, such as those found in Vemurafenib and Pexidartinib, show promise as anticancer agents. Additionally, pyrrolo[3,2-*c*]pyridine derivatives have displayed inhibitory effects on FMS kinase, making them potential candidates for anticancer and antiarthritic drugs development.[10]

In terms of pharmacological targets, pyridine and its precursor, dihydropyridine, are ubiquitous structural elements. These ring systems have made significant contributions to drug design, leading to the development of numerous broad-spectrum therapeutic medicines. Over 95 approved pharmaceuticals in the US FDA database are derived from pyridine or dihydropyridine, including drugs for tuberculosis, HIV/AIDS, cancer, Alzheimer's, arthritis, hypertension, and more.[11]

At the same time, some ortho-diphenols have shown antioxidant properties, which are valuable in protecting cells from oxidative stress and damage caused by free radicals. For example, certain plant-derived ortho-diphenols, such as catechins found in green tea, have been investigated for their antioxidant effects and potential health benefits. Moreover, some ortho-diphenols have demonstrated antibacterial and antifungal properties, making them potentially useful in the development of antimicrobial agents.

Given the information discussed above, the focus of our current study is to synthesize new derivatives, building upon our previous research on N-heterocycle systems,[12–14] while remaining aligned with our keen interest in exploring chemical compounds with physiological activity.[15–19]

This article presents our findings, including the synthesis, characterization, and antitumor evalution of several new N-heterocycle monoquaternary salts. Additionaly, we discuss two unexpected physical mixtures that formed during the process (Fig. 1).

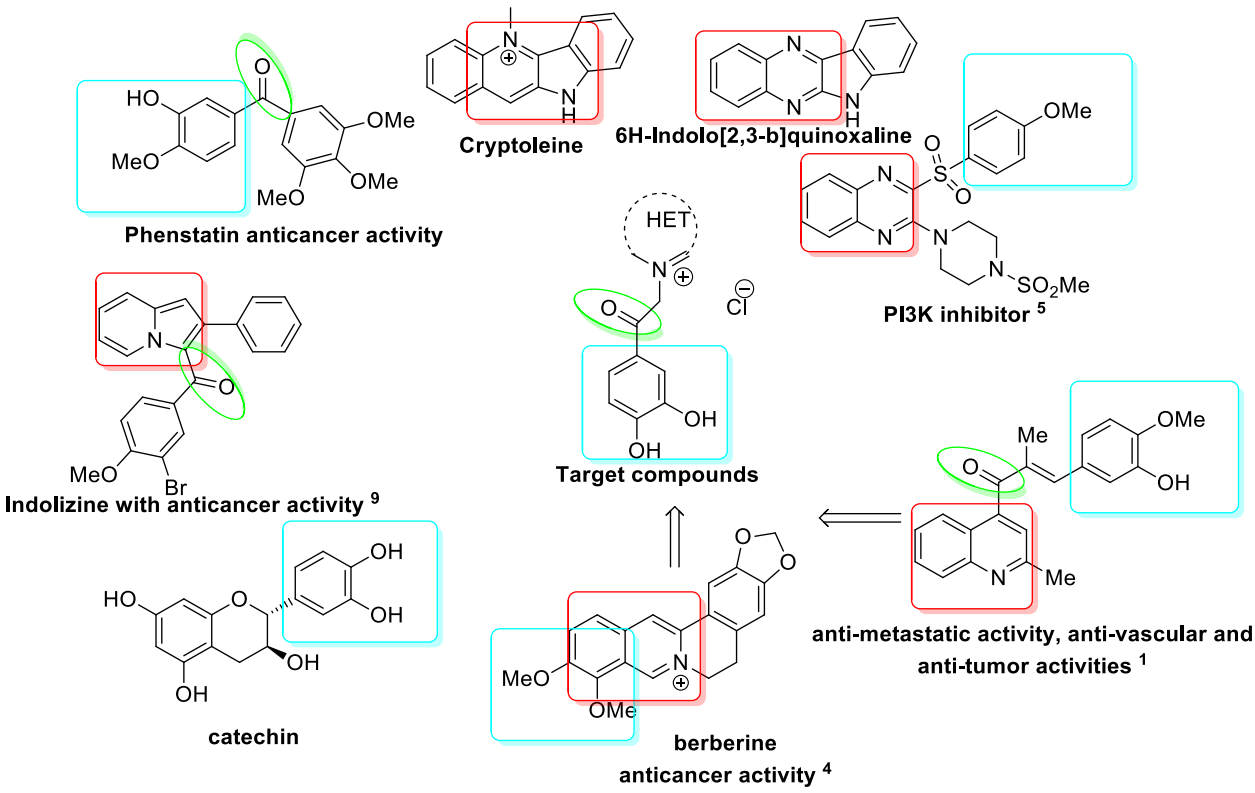

Fig. 1 – Design strategy in current synthesis.

RESULTS AND DISCUSSION

Chemistry

As depicted in Scheme 1, the synthesis of monoquaternary salts **3a-f** involved the direct reaction between the corresponding N-heterocycle **1** and 2-chloro-1-(3,4-dihydroxyphenyl)ethanone **2** in acetone under reflux conditions.[20,21] In these conditions, once formed, the monoquaternary salts precipitate and they are filtered off from the reaction mixtures.

Under the same reaction conditions, starting compounds **1g** and **1h** did not yield the desired monoquaternary salts as expected. Even though the reactions seemed to proceed similarly, yielding a stable precipitate that was then filtered off. Instead, spectral data showed that we obtained a physical mixture of reactants, where the hydroxyl moiety from 2-chloro-1-(3,4-dihydroxyphenyl)ethanone **2** was oriented at the nitrogen in quinoline or quinoxaline. This orientation effectively hindered the formation of the intended compounds.

Regardless of the reaction conditions attempted (other solvents such as acetonitrile see Figure S9 and S11, ultrasounds, microwave, solventless, etc), we were unable to obtain the corresponding monoquaternary salts; instead, we only obtained physical mixtures of **3g** and **3h**.

The structures of all synthesized compounds were fully confirmed using ^{1}H and ^{13}C-NMR (see Supporting Information). More deep information about proton-proton and proton-carbon spin systems was obtained from homo- and heteronuclear bidimensional correlation experiments like ^{1}H, ^{1}H-COSY, ^{1}H-^{13}C-HSQC and ^{1}H-^{13}C-HMBC, IR, and MS analysis. Additionally, the **3g** mixture successfully crystallized, enabling us to elucidate the interaction between the two molecules via XRD.

Thus, according to the single crystal X-ray diffraction study, mixture **3g** exhibits a molecular crystal structure that arises from the co-crystallization of two neutral entities: quinoline **1g** and 2-chloro-1-(3,4-dihydroxyphenyl)ethanone **2** in 1:1 ratio. All the components of the structure are interconnected via O-H···O and O-H···N hydrogen bonding to form a supramolecular associate, as shown in Fig. 2.

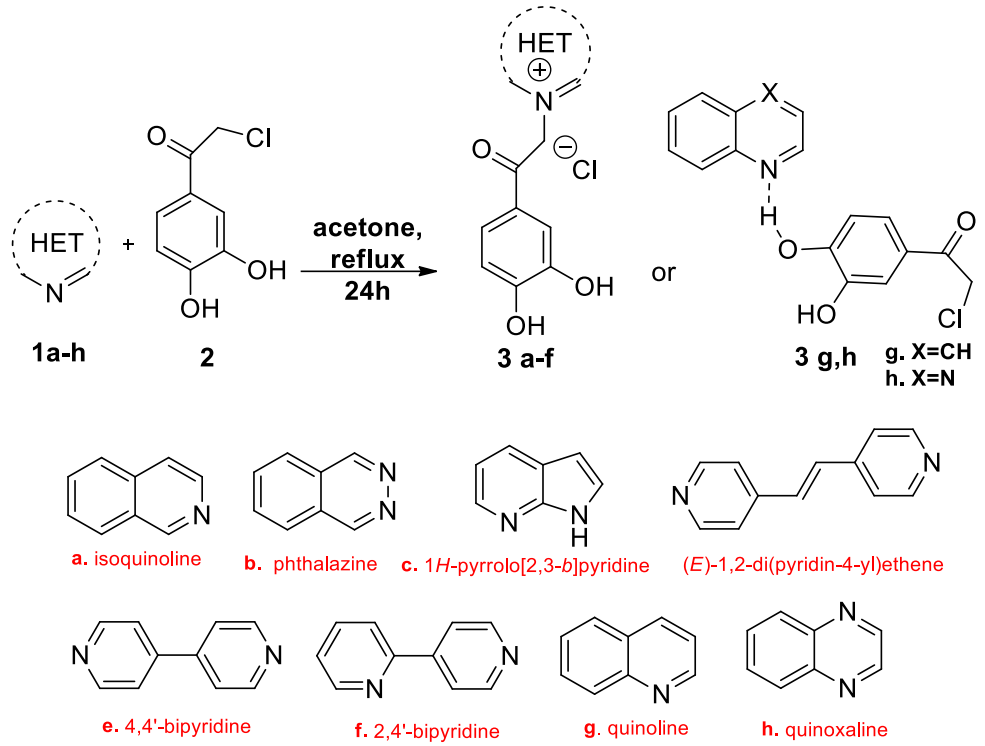

Scheme 1 – Synthetic pathway for obtaining monoquaternary salts 3a–f, and physical mixtures 3g and 3h.

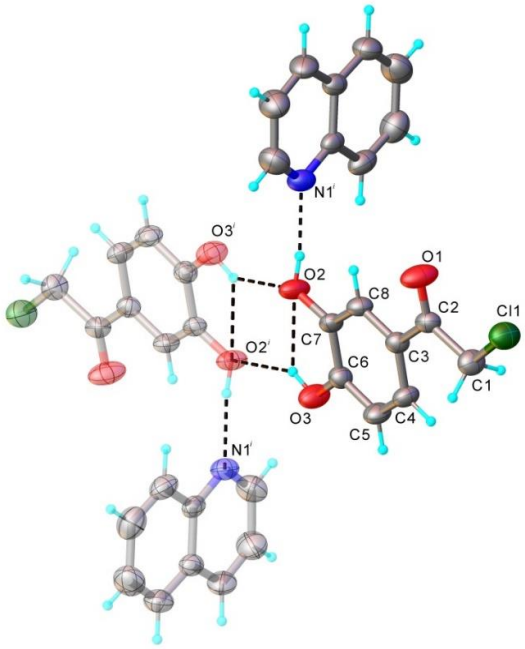

Fig. 2 – Extended view of the symmetric part in the crystal structure of **3g** mixture with atom labeling scheme and thermal ellipsoids at 50% level. Symmetry generated fragments are shown with faded colours. (H-bonds parameters: O2-H---N1 [O2-H 0.82 Å, H···N1 1.84 Å, O2···N1 2.659(2) Å, ∠O1HN1 172.5°; O3-H---O2 [O3-H 0.82 Å, H···O2 2.30 Å, O3···O2 2.739(2) Å, ∠O1HO2 113.7°; O3-H---O2 [O3-H 0.82 Å, H···O2 2.04 Å, O3···O2(–*x*, 1 – *y*, 1 – *z*) 2.721(2) Å, ∠O3HO2 140.2°.)

Further analysis indicated that the crystal packing is driven by π-π stacking interactions between aromatic rings of quinoline and 2-chloro-1-(3,4-dihydroxyphenyl)ethanone molecules, which determine the formation of a 3D supramolecular network, as shown in Fig. 3.

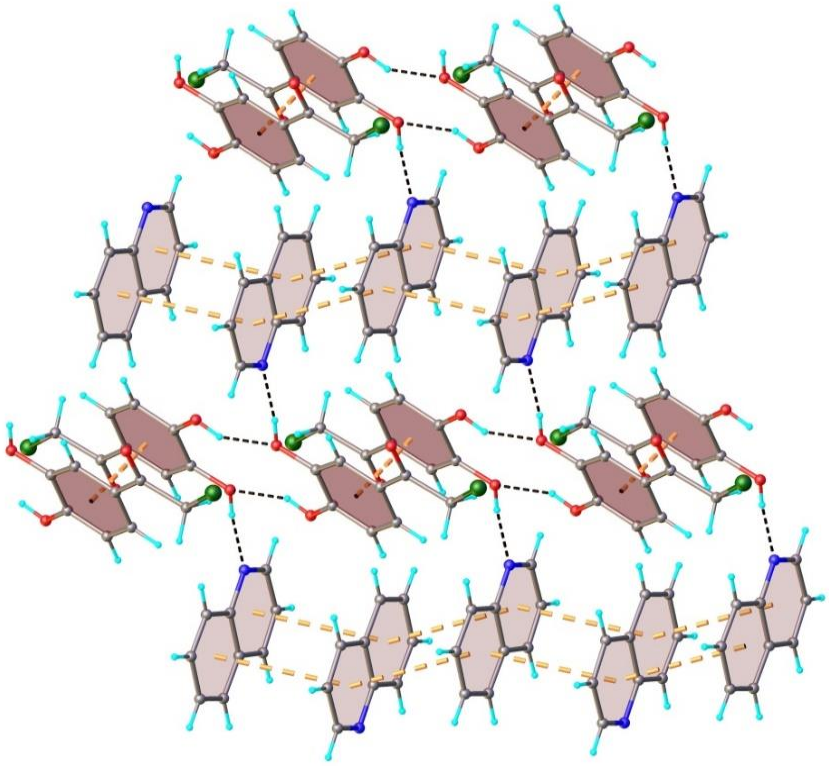

Fig. 3 – View of 3D supramolecular network in the crystal structure of mixture **3g**. H bonds and centroid-to-centroid distances are drawn in dashed black and orange lines, respectively. Centroid-to-centroid distances are of 3.711(4) and 3.897(3) Å.

Biological activity-anticancer activity

NCI testing on 60 human tumor cell lines

The synthesized substances were submitted and selected for evaluation by the National Cancer Institute (NCI). Quaternary salts **3a–f** and the mixtures **3g–h** were subjected to single-dose screening (10^{-5} M) against a panel of 60 human tumor cell lines, encompassing leukemia, melanoma, lung, colon, central nervous system, ovary, kidney, prostate, and breast cancers. Table 1 presents representative outcomes of the tested chemicals.

Table 1

Results of the *in vitro* growth inhibition (GI%) of tested compounds against human cancer cell lines in the single dose assay[a]

Cell type	Cell line	GI (%) (10^{-5}M)[a]							
	Compund	**3a**	**3b**	**3c**	**3d**	**3e**	**3f**	**3g**	**3h**
Leukemia	CCRF-CEM	2	0	1	63	3	6	**100**[c]	**95**
	K-562	5	3	0	68	0	0	72	83
	SR	0	0	0	62	0	0	92	93
	HL-60(TB)	2	4	0	37	1	0	**100**[d]	**100**[f]
	MOLT-4	0	0	0	42	0	0	**93**	88
Non-small Cell Lung Cancer	A549/ATCC	54	1	0	0	0	0	16	13
	EKVX	15	0	1	1	3	0	23	6
	HOP-92	0	7	0	11	2	0	27	35
	NCI-H226	0	9	0	7	0	0	38	29
	NCI-H460	0	0	0	1	0	0	7	29
	NCI-H522	14	10	0	46	5	0	79	**100**[g]
Colon Cancer	COLO205	0	0	0	10	0	0	44	69
	HCT-116	1	0	0	32	0	1	**95**	**93**
	HCT-15	0	2	0	61	0	0	79	87
	HT-29	1	0	0	13	0	0	69	82
	SW-620	-	6	1	45	1	0	84	76
	KM12	2	0	0	0	0	0	0	18

(*Table 1 continues*)

(*Table 1 continues*)

Cell type	Cell line Compund	GI (%) (10^{-5}M)[a]							
		3a	**3b**	**3c**	**3d**	**3e**	**3f**	**3g**	**3h**
CNS Cancer	SF-268	17	0	0	6	0	0	15	14
	SF-539	4	0	0	4	0	0	9	47
	SNB-75	7	0	0	0	1	0	35	2
	U251	0	0	0	1	0	0	9	36
	SNB-19	0	9	0	1	1	0	26	19
Melanoma	LOX IMVI	11	6	0	32	0	3	82	**91**
	M14	4	2	6	13	2	5	**100**[e]	39
	UACC-62	3	6	5	13	5	3	50	45
	UACC-257	0	0	0	21	0	0	22	42
Ovarian Cancer	OVCAR-3	0	0	0	45	0	0	66	78
	NCI/ADR-RES	2	2	0	3	0	0	25	43
	IGROV1	3	0	0	10	0	0	51	49
	OVCAR-8	0	2	0	8	0	0	51	52
	OVCAR-4	6	5	0	25	0	0	45	53
Renal cancer	A498	0	0	0	0	0	2	12	12
	RXF393	0	10	0	23	0	0	50	83
	ACHN	0	0	0	32	0	0	76	82
	UO-31	30	13	7	19	9	7	50	60
	TK10	11	0	1	13	5	7	61	57
Breast cancer	MCF7	0	9	0	48	3	2	78	87
	MDA-MB-468	7	4	0	50	0	0	84	45
	T-47D	1	0	0	16	0	0	58	55
	MDA-MB-231/ATCC	2	7	0	9	3	1	41	45
	BT-549	0	0	0	14	0	0	35	48
Prostate cancer	PC-3	17	8	0	12	7	0	30	55
	DU-145	1	0	0	10	0	0	15	53

[a] Data obtained from NCI's *in vitro* 60 cell one dose screening at 10^{-5}M concentration; [b] Cytotoxic effect; Cell growth percent: [c] –14; [d] –20; [e] –83; [f] –25; [g] –5. The best values in terms of growth inhibition are highlighted in bold and red or blue.

Surprisingly, out off all tested derivatives, physical mixtures **3g** and **3h** showed the best efficacy in terms of growth inhibition of several cancer cell lines.

The best results were shown by mixture **3g** against the HL-60(TB) and CCRF-CEM, SR and MOLT-4 leukemia cell lines and M14 melanoma cell lines, but also against HCT-116 colon cancer cell line. Regarding compound **3h**, it possessed a very good activity against the HL-60(TB) and CCRF-CEM and SR leukemia cell lines, also against HCT-116 (colon cancer) NCI-H522 (non-small cell lung cancer).

In the series of monoquaternary salts, only (*E*)-1-(2-(3,4-dihydroxyphenyl)-2-oxoethyl)-4-(2-(pyridin-4-yl)vinyl)pyridin-1-ium chloride **3d** showed moderate inhibitory activity especially against leukemia cells, but also on HCT-15 (colon cancer) and MDA-MB-468 (breast cancer).

MTS assay on MCF7 breast cancer cell

To evaluate the antitumor activity of mixtures **3g** and **3h**, we conducted cytotoxicity assays on normal fibroblasts and MCF7 breast cancer cell lines over 24 hours of incubation, comparing them with the starting materials, quinoline, and quinoxaline, respectively. We selected the MCF7 breast cancer cell line because both **3g** and **3h** samples exhibited promising activity (78% for **3g** and 87% for **3h**) in previous tests conducted by the National Cancer Institute (NCI). The compounds were initially tested at an equivalent concentration to that employed in NCI studies (10^{-5} M). However, no discernible activity was observed. The discrepancy between the NCI results and the MTS assay could be attributed to differences in experimental protocols and working procedures. Subsequently, in this instance, the compounds underwent testing at concentrations of 2.5×10^{-5} M, 5×10^{-5} M, 7.5×10^{-5} M and 10^{-4} M. Furthermore, we calculated the compounds' concentration that induce 50% decrease in cell viability (IC_{50}) for each cell line.

Figure 4 illustrates the cytotoxicity of the compounds on normal fibroblasts (Fig. 4a) and MCF7 breast cancer cells (Fig. 4b). We can observe from Fig. 4a that quinoline and quinoxaline were biocompatible at the tested concentrations, while compound **2** induced cytotoxicity in normal fibroblasts at concentrations above 5×10^{-5} M (IC_{50} = 6.11×10^{-5} M). Also, we can observe an amplified cytotoxic effect of the mixtures **3g** and **3h**, demonstrated by significantly lower IC_{50} values: 3.51×10^{-5} M and 3.24×10^{-5} M, respectively.

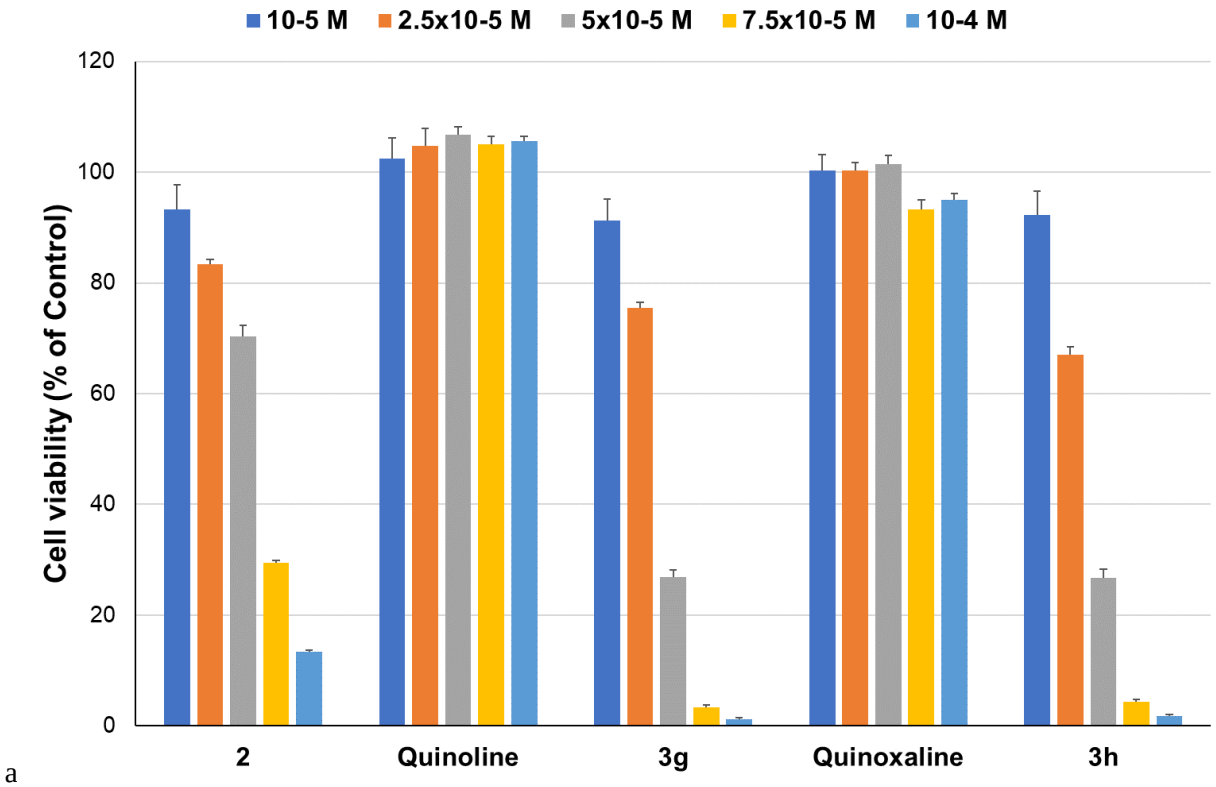

a

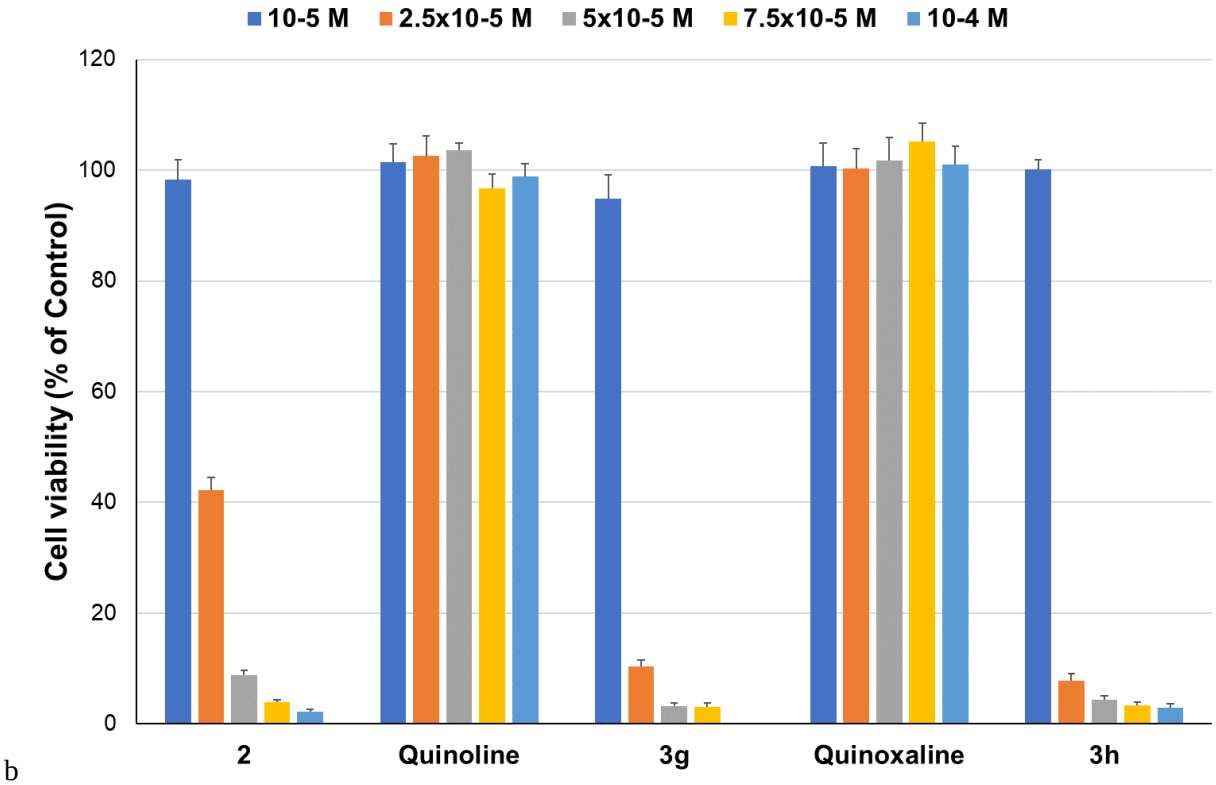

b

Fig. 4 – Cell viability of a) normal fibroblasts and b) MCF7 breast cancer cells after 24 hours of incubation with tested compounds

We can observe from Fig. 4b that quinoline and quinoxaline were non-cytotoxic to MCF7 cells as well at the tested concentrations. Compound **2** had a pronounced cytotoxic effect on MCF7 cells compared to normal fibroblasts, demonstrated by its IC_{50} = 2.32×10^{-5} M, which is 2.6 times lower

than the IC_{50} for normal fibroblasts. The amplified cytotoxic effect of the mixtures **3g** and **3h** was also noted on MCF7 cells, with IC_{50} values of 1.69×10^{-5} M and 1.93×10^{-5} M, respectively.

To summarize the cytotoxicity results, we can say that the optimal concentration of compound **2** would be 5×10^{-5} M, while for mixtures **3g** and **3h** effective antitumoral activity could be achieved with 2.5×10^{-5} M.

Improved molecular interactions with the target biomolecules may arise from the hydrogen bonds that form between quinoline and quinoxaline, respectively, in the mixture containing 2-chloro-1-(3,4-dihydroxyphenyl)ethenone **2**. Better binding affinity and biological activity against the tumor cells may follow from this.

EXPERIMENTAL

Chemistry

Without additional filtration, all commercially available reagents and solvents were utilized. The uncorrected melting points were obtained using an A. Krüss Optronic Melting Point Meter KSPI. Commercial silica gel plates 60 F254 (Merck Darmstadt, Germany) were used for analytical thin-layer chromatography, which was then observed under UV light (max = 254 or 365 nm). The NMR spectra were captured using an Avance III 500 MHz spectrometer from Bruker Vienna, Austria, which operates at 125 MHz for ^{13}C and 500 MHz for ^{1}H. Chemical shifts were given as part per million (ppm), coupling constants (*J*) in Hz, and delta (δ) units. Chemical shift multiplicities were denoted by the following abbreviations: s = singlet, d = doublet, t = triplet, q = quartet, m = multiplet, and bs = broad singlet. H,H-COSY (Correlation Spectroscopy), H,C-HSQC (Heteronuclear Single Quantum Coherence) and H,C-HMBC (Heteronuclear Multiple Bond Correlation) experiments were recorded using standard pulse sequences as delivered by Bruker with TopSpin 4.0.8 spectrometer control and processing software. IR spectra were recorded on a Shimadzu IRTracer-100 instrument (Shimadzu U.S.A. Manufacturing, Inc., Canby, OR, USA). The analyses that the elements' or functions' symbols denoted were within 0.4% of the theoretical values. Mass spectra were acquired on a Bruker Rapiflex MALDI-TOF (Bruker Daltonics, Bremen-GERMANY) equipped with a Smartbeam 3D laser. The samples were dissolved in DMSO and then diluted 10 times in methanol. For the MALDI matrix solutions, 20 mg of α-cyano-4-hydroxycinnamic acid (HCCA) was dissolved in 1ml methanol. Then, MALDI matrix solution and sample solution was mixed each other in 1:1, 2:1 and 4:1 ration and finally 1 µL from each final solution was deposited onto the MALDI target, dried at room temperature and analyzed in MALDI-TOF-MS. Mass calibration of MALDI-TOF-MS was performed by the peptide mixture standard solution (Bruker Daltonics, Bremen-GERMANY). FlexControl (Bruker Daltonics, Version 4.0) was used to optimize and acquire data using the following parameters: positive ion polarity in reflector mode, mass scan range m/z 100–1600 Da), digitizer 1.25 GHz, detector voltage 2117 V, 1000 shots per pixel, and 5 kHz laser frequency. The laser power was set at 60% to 80% of the maximum and 1000 laser shots were accumulated for each spectrum. The MS/MS fragmentation experiments were performed in LIFT mode using a Bruker standard fragmentation method.

***General procedure for synthesis of monoquaternary salts* 3a-f *and physical mixtures* 3g *and* 3h**

The corresponding *N*-heterocycle **1** (isoquinoline **a,** phthalazine **b,** pyrrolopyridine **c,** transetylene-bylpyridine **d,** 4,4'-bipyridine **e,** 2,4'-bipyridine **f,** quinoline **g,** quinoxaline **h**) (1 mmol, 1 equiv.) was dissolved in 5-7 mL acetone. Then, 2-chloro-(3,4-dihydroxyphenyl)ethanone **2**, (1.1 mmol, 1.1 equiv.) was added and the resulting mixture was stirred overnight at reflux. The formed precipitate was filtered and washed with acetone to give the desired product.

***2-(2-(3,4-dihydroxyphenyl)-2-oxoethyl)isoquinolin-2-ium chloride* (3a):**

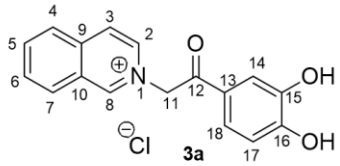

Brown solid, η=95%, m.p.= 215–217 °C. IR ATR ν(cm^{-1}): 3126, 2057, 2860, 2722, 2362, 2160, 1684, 1642, 1595, 1515, 1473, 1395, 1332, 1279, 1170, 1121, 911, 798, 620, 466. ^{1}H NMR (DMSO-d_6, 500 MHz): δ= 6.53 (s, 2H, H_{11}), 7.03 (d, *J*= 8.0 Hz, 1H, H_{17}), 7.49 (s, 1H, H_{14}), 7.52 (d, *J*= 8.0 Hz, 1H, H_{18}), 8.10 (t, *J*= 7.5 Hz, 1H, H_6), 8.32 (t, *J*= 7.5 Hz, 1H, H_5), 8.40 (d, *J*= 8.5 Hz, 1H, H_4), 8.53 (d, *J*= 8.5 Hz, 1H, H_7), 8.66 (d, *J*= 6.5 Hz, 1H, H_3), 8.74 (d, *J*= 6.5 Hz, 1H, H_2), 9.74 (s, 1H, OH), 10.08 (s, 1H, H_8), 10.45 (s, 1H, OH). ^{13}C NMR (DMSO-d_6, 125 MHz): δ= 65.6 (C_{11}), 115.1 (C_{14}), 115.6 (C_{17}), 121.9 (C_{18}), 125.2 (C_{13}), 125.4 (C_3), 126.9 (C_{10}), 127.4 (C_4), 130.6 (C_7), 131.4 (C_6), 136.4 (C_2), 137.2 (C_9), 137.4 (C_5), 145.8 (C_{15}), 151.7 (C_8), 152.4 (C_{16}), 188.8 (C_{12}). MS (positive mode): m/z calcd for $[M\text{-}Cl]^+$ 280.10, found 280.06.

***2-(2-(3,4-dihydroxyphenyl)-2-oxoethyl)phthalazin-2-ium chloride* (3b):**

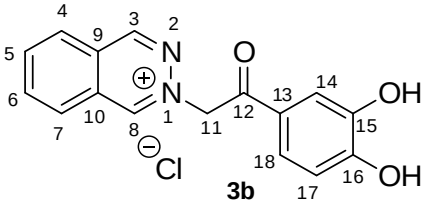

Brown solid, η=89%, m.p. 221–223 °C. IR ATR ν(cm^{-1}): 3128, 2056, 2862, 2721, 2361, 2159, 1686, 1643, 1593, 1512, 1474, 1395, 1333, 1278, 1172, 1122, 912, 798, 622, 466. ^{1}H NMR (500MHz, DMSO-d_6): δ= 6.67 (s, 2H, H_{11}), 7.04 (d, *J*= 8.5 Hz, 1H, H_{17}), 7.35 (as, 1H, H_{14}), 7.57 (d, *J*= 8.0 Hz, 1H, H_{18}), 8.46 (t, *J*= 8.0 Hz, 1H, H_6), 8.57 (t, *J*= 7.5 Hz, 1H, H_5), 8.66 (d, *J*= 8.0 Hz, 1H, H_4), 8.72 (d, *J*= 8.0 Hz, 1H, H_7), 9.77 (s, 1H, OH), 10.21 (s, 1H, H_3), 10.59 (s, 1H, OH), 10.83 (s, 1H, H_8). ^{13}C NMR (125 MHz, DMSO-d_6): δ = 68.4 (C_{11}), 115.2 (C_{14}), 115.7 (C_{17}), 122.3 (C_{18}), 125.1 (C_{10}), 127.2 (C_9), 127.4 (C_{13}), 128.6 (C_4), 130.7 (C_7), 136.5 (C_6), 139.8 (C_5), 145.9 (C_{15}), 152.7 (C_{16}), 153.5 (C_8), 154.8 (C_3), 188.4 (C_{12}). MS (positive mode): m/z calcd for $[M\text{-}Cl]^+$ 281.09, found 281.08.

***7-(2-(3,4-dihydroxyphenyl)-2-oxoethyl)-1H-pyrrolo[2,3-b]pyridin-7-ium chloride* (3c):**

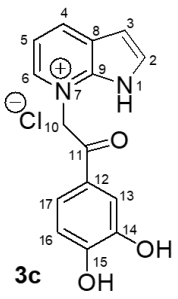

Brown solid, η=89%, m.p. 287–289 °C. IR ATR ν(cm^{-1}): 3674, 2988, 2900, 2717, 2357, 1678, 1622, 1599, 1516, 1394, 1360, 1338, 1290, 1186, 1149, 1064, 1010, 883, 781, 719, 628, 468. ^{1}H-NMR (500MHz, DMSO-d$_6$): 6.51 (s, 2H, H$_{10}$), 6.98–7.01 (overlapped signals, 2H, H$_3$, H$_{16}$), 7.46 (s, 1H, H$_{13}$), 7.50 (d, *J*= 8.5 Hz, 1H, H$_{17}$), 7.70 (dd, *J*= 7.5; 6.5 Hz, 1H, H$_5$), 7.92 (d, *J*= 3.0 Hz, 1H, H$_2$), 8.61 (d, *J*= 6.0 Hz, 1H, H$_6$), 8.81 (d, *J*= 8.0 Hz, 1H, H$_4$), 9.67 (s, 1H, OH), 10.35 (s, 1H, OH). ^{13}C-NMR (125 MHz, DMSO-d$_6$): 61.4 (C$_{10}$), 103.5 (C$_3$), 115.2 (C$_{13}$), 115.5 (C$_{16}$), 116.1 (C$_5$), 122.0 (C$_{17}$), 125.4 (C$_{12}$), 126.6 (C$_8$), 130.1 (C$_2$), 137.8 (C$_6$), 137.9 (C$_4$), 140.1 (C$_9$), 145.6 (C$_{14}$), 152.2 (C$_{15}$), 188.1 (C$_{11}$). MS (positive mode): m/z calcd for [M-Cl]$^+$ 269.09, found 269.07.

***(E)-1-(2-(3,4-dihydroxyphenyl)-2-oxoethyl)-4-(2-(pyridin-4-yl)vinyl)pyridin-1-ium chloride* (3d):**

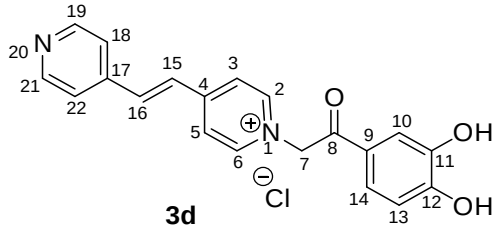

White solid, η = 90%, m.p.= 289–291 °C. IR ATR ν(cm^{-1}): 2930, 1684, 1639, 1593, 1518, 1342, 1285, 1173, 1124. ^{1}H-NMR (500MHz, DMSO-d$_6$): δ= 6.30 (s, 2H, H$_7$), 6.98 (d, *J*= 8.0 Hz, 1H, H$_{13}$), 7.44 (d, *J*= 2.0 Hz, 1H, H$_{10}$), 7.48 (dd, *J*= 8.5; 2.0 Hz, 1H, H$_{14}$), 7.70 (d, *J*= 5.5 Hz, 2H, H$_{18}$, H$_{22}$), 7.84 (d, *J*= 16.5 Hz, 1H, H$_{15}$), 8.03 (d, *J*= 16.5 Hz, 1H, H$_{16}$), 8.39 (d, *J*= 7.0 Hz, 2H, H$_3$, H$_5$), 8.71 (d, *J*= 5.5 Hz, 2H, H$_{19}$, H$_{21}$), 8.93 (d, *J*= 7.0 Hz, 2H, H$_2$, H$_6$), 9.68 (s, 1H, OH), 10.38 (s, 1H, OH). ^{13}C-NMR (125 MHz, DMSO-d$_6$): δ= 65.1 (C$_7$), 115.0 (C$_{10}$), 115.6 (C$_{13}$), 121.8 (C$_{14}$), 121.9 (C$_{18}$, C$_{22}$), 124.3 (C$_3$, C$_5$), 125.2 (C$_9$), 127.9 (C$_{15}$), 138.3 (C$_{16}$), 142.2 (C$_{17}$), 145.7 (C$_{11}$), 146.2 (C$_2$, C$_6$), 150.6 (C$_{19}$, C$_{21}$), 152.3 (C$_{12}$), 152.4 (C$_4$), 188.7 (C$_8$). MS (positive mode): m/z calcd for [M-Cl]$^+$ 333.12, found 333.10.

***1-(2-(3,4-dihydroxyphenyl)-2-oxoethyl)-[4,4'-bipyridin]-1-ium chloride* (3e):**

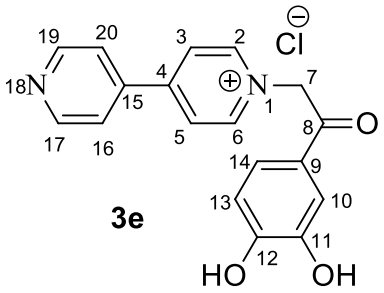

Brown solid., η= 76%, m.p.= 310–311 °C. IR ATR ν(cm^{-1}): 3674, 2985, 2900, 2750, 1672, 1641, 1589, 1521, 1456, 1409, 1328, 1301, 1242, 1215, 1188, 1110, 1066, 1010, 877, 813, 796, 644, 511. ^{1}H-NMR (500MHz, DMSO-d$_6$): δ= 6.38 (s, 2H, H$_7$), 6.98 (d, *J*= 6.5 Hz, 1H, H$_{13}$), 7.45 (s, 1H, H$_{10}$), 7.50 (d, *J*= 6.5 Hz, 1H, H$_{14}$), 8.09 (bs, 2H, H$_{16}$, H$_{20}$), 8.72 (bs, 2H, H$_3$, H$_5$), 8.96 (bs, 2H, H$_{17}$, H$_{19}$), 9.12 (bs, 2H, H$_2$, H$_6$), 9.68 (s, 1H, OH), 10.38 (s, 1H, OH). ^{13}C-NMR (125 MHz, DMSO-d$_6$): δ= 65.4 (C$_7$), 114.9 (C$_{10}$), 115.6 (C$_{13}$), 121.9 (C$_{14}$), 122.2 (C$_{16}$, C$_{20}$), 125.1 (C$_3$, C$_5$, C$_9$), 140.9 (C$_{15}$), 146.8 (C$_2$, C$_6$), 145.8 (C$_{11}$), 151.0 (C$_{17}$, C$_{19}$), 152.4 (C$_{12}$), 152.9 (C$_4$), 188.5 (C$_8$). MS (positive mode): m/z calcd for [M-Cl]$^+$ 307.11, found 307.05.

***1'-(2-(3,4-dihydroxyphenyl)-2-oxoethyl)-[2,4'-bipyridin]-1'-ium chloride* (3f):**

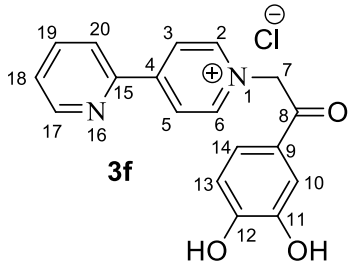

Yellow solid, η= 82%, m.p.= 301–302 °C. %. IR ATR ν(cm^{-1}): 3674, 3647, 3568, 3225, 2972, 2900, 2362, 1681, 1637, 1587, 1518, 1458, 1337, 1288, 1275, 1170, 1123, 773, 617, 578. ^{1}H-NMR (500MHz, DMSO-d$_6$): δ= 6.45 (s, 2H, H$_7$), 7.03 (d, *J*= 8.5 Hz, 1H, H$_{13}$), 7.49–7.51 (overlapped signals, 2H, H$_{10}$, H$_{14}$), 7.70 (dd, *J*= 8.0; 4.5 Hz, 1H, H$_{18}$), 8.15 (td, *J*= 9.0; 1.5 Hz, 1H, H$_{19}$), 8.49 (d, *J*= 8.0 Hz, 1H, H$_{20}$), 8.90-8.91 (overlapped signals, 3H, H$_{17}$, H$_3$, H$_5$), 9.12 (d, *J*= 7.0 Hz, 2H, H$_2$, H$_6$), 9.76 (s, 1H, OH), 10.49 (s, 1H, OH). ^{13}C-NMR (125 MHz, DMSO-d$_6$): δ= 65.3 (C$_7$), 115.1 (C$_{10}$), 115.6 (C$_{13}$), 121.8 (C$_{14}$), 123.6 (C$_{20}$), 124.0 (C$_3$, C$_5$), 125.1 (C$_9$), 126.7 (C$_{18}$), 138.3 (C$_{19}$), 146.8 (C$_2$, C$_6$), 145.8 (C$_{11}$), 149.8 (C$_{15}$), 150.8 (C$_{17}$), 152.4 (C$_{12}$), 153.3 (C$_4$), 188.7 (C$_8$). MS (positive mode): m/z calcd for [M-Cl]$^+$ 307.11, found 307.08.

***H*-bonded physical mixture quinoline / 2-chloro-1-(3,4-dihydroxyphenyl)ethanone* (3g):**

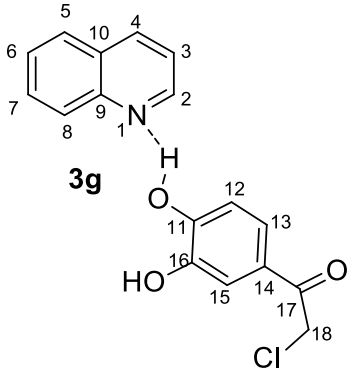

Brown solid, η =89%, p.t. = 221–223 ºC; %. IR ATR ν(cm^{-1}): 3024, 2956, 1673, 1598, 1519, 1359, 1240, 1175. ^{1}H NMR (DMSO-d$_6$, 500 MHz): δ= 5.02 (s, 2H, H$_{18}$), 6.83 (d, *J* = 8.0 Hz, 1H, H$_{12}$), 7.35 (s, 1H, H$_{15}$), 7.38 (d, *J* = 8.0 Hz, 1H, H$_{13}$), 7.54 (m, 1H, H$_3$), 7.62 (t, *J* = 7.0 Hz, 1H, H$_6$), 7.77 (t, *J* = 7.0 Hz, 1H, H$_7$), 7.99 (d, *J* = 8.0 Hz, 1H, H$_5$), 8.02 (d, *J* = 8.5 Hz, 1H, H$_8$), 8.37 (d, *J* = 7.5 Hz, 1H, H$_4$), 8.91 (bs, 1H, H$_2$), 9.75 (bs, 2H, 2 x OH). ^{13}C NMR (DMSO-d$_6$, 125 MHz): δ= 47.1 (C$_{18}$), 115.2 (C$_{13}$, C$_{15}$), 121.5 (C$_3$), 121.9 (C$_{12}$), 126.1 (C$_{11}$), 126.6 (C$_6$), 127.9 (C$_9$), 128.1 (C$_5$), 128.9 (C$_8$), 129.5 (C$_7$), 136.0 (C$_2$), 145.4 (C$_{14}$), 147.7 (C$_{10}$), 150.6 (C$_4$), 151.4 (C$_{16}$), 189.7 (C$_{17}$).

***H-bonded physical mixture quinoxaline /2-chloro-1-(3,4-dihydroxyphenyl)ethenone* (3h):**

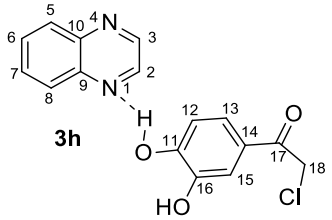

Brown solid, yield: 67%, mp = 172–173°C. IR ATR ν(cm^{-1}): 3125, 2056, 2858, 2720, 2360, 2159, 1686, 1643, 1597, 1512, 1470, 1392, 1330, 1281, 1171, 1120, 915, 799, 622, 467. ^{1}H NMR ($CDCl_3$, 500 MHz, δ(ppm)): 5.01 (s, 2H, H_{18}), 6.82 (d, J = 8.5 Hz, 1H, H_{12}), 7.34 (s, 1H, H_{15}), 7.36 (d, J = 8.5 Hz 1H, H_{13}), 7.88 (d, J = 3.5 Hz, 2H, $H_{6,}$ H_7), 8.12 (d, J = 3.5 Hz, 2H, $H_{5,}$ H_8), 8.96 (s, 2H, $H_{2,}$ H_3), 9.44 (s, 1H, OH), 10.04 (s, 1H, OH). ^{13}C NMR (DMSO-d_6, 125 MHz): δ= 47.1 (C_{18}), 115.2 (C_{12}), 121.9 (C_{15}), 126.1 (C_{13}), 129.2 ($C_{6,}$ C_7), 130.3 ($C_{5,}$ C_8), 142.3 (C_{14}), 145.4 (C_{16}), 145.8 ($C_{2,}$ C_3), 151.4 (C_{11}), 189.7 (C_{17}).

X-ray Diffraction

Single-crystal X-ray diffraction data were collected on an Oxford-Diffraction XCALIBUR Eos CCD diffractometer with graphite-monochromated Mo-Kα radiation. The unit cell determination and data integration were carried out using the CrysAlisPro package from Oxford Diffraction.[22] Multi-scan correction for absorption was applied. The structures were solved with program SHELXT using the intrinsic phasing method and refined by the full-matrix least-squares method on F^2 with SHELXL.[23,24] Olex2 was used as an interface to the SHELX programs.[25] Non-hydrogen atoms were refined anisotropically. Hydrogen atoms were located in idealized positions and refined using a riding model. Selected crystallographic data and structure refinement details are provided in Table 2. Bond distances and angles are summarized in Table 3.

Table 2

Crystal data and details of structure refinement

Emp. formula	$C_{17}H_{14}ClNO_3$
F_w	315.74
T [K]	293
space group	P-1
a [Å]	7.5898(6)
b [Å]	8.3192(7)
c [Å]	11.7066(11)
α [°]	83.988(7)
β [°]	83.172(7)
γ [°]	86.807(6)
V [Å^3]	729.19(11)
Z	2
ρ_{calcd} [g cm^{-3}]	1.438
μ [mm^{-1}]	0.274
Crystal size [mm]	0.15 × 0.05 × 0.05
2Θ range	4.928 to 50.054
Refls. collected	3906
Indep. Refls., R_{int}	3906, 0.0497
Data/rests./params.	3906/0/202
GOF	1.037
$R_{1,}$ wR_2(all data)	0.0363, 0.0606
CCDC no.	2277786

Table 3

Bond distances (Å) and angles (°)

Cl1-C1	1.7700(19)
O1-C2	1.208(2)
O2-C7	1.361(2)
O3-C6	1.360(2)
C1-C2	1.514(3)
C2-C3	1.473(3)
C3-C4	1.389(3)
C3-C8	1.389(3)
C4-C5	1.380(3)
C5-C6	1.371(3)
C6-C7	1.398(2)
C7-C8	1.379(3)
N1-C9	1.306(3)
N1-C17	1.369(3)
C9-C10	1.401(3)
C10-C11	1.351(3)
C11-C12	1.397(3)
C12-C13	1.405(3)
C12-C17	1.421(3)
C13-C14	1.350(3)
C14-C15	1.404(3)
C15-C16	1.357(3)
C16-C17	1.400(3)
C2-C1-Cl1	113.37(14)
O1-C2-C1	121.0(2)
O1-C2-C3	122.9(2)
C3-C2-C1	116.08(18)
C4-C3-C2	122.2(2)
C4-C3-C8	118.7(2)
C8-C3-C2	119.05(19)
C5-C4-C3	120.1(2)
C6-C5-C4	120.9(2)
O3-C6-C5	117.95(19)
O3-C6-C7	122.3(2)
C5-C6-C7	119.8(2)
O2-C7-C6	116.82(19)
O2-C7-C8	124.13(18)
C8-C7-C6	119.0(2)
C7-C8-C3	121.37(19)
C9-N1-C17	117.84(18)
N1-C9-C10	124.6(2)
C11-C10-C9	118.0(2)
C10-C11-C12	120.5(2)
C11-C12-C13	124.3(2)

(*Table 3 continues*)

(*Table 3 continues*)

Bond distances (Å) and angles (°)

C11-C12-C17	117.5(2)
C13-C12-C17	118.2(2)
C14-C13-C12	121.4(2)
C13-C14-C15	120.2(2)
C16-C15-C14	120.3(2)
C15-C16-C17	120.7(2)
N1-C17-C12	121.4(2)
N1-C17-C16	119.36(19)
C16-C17-C12	119.2(2)

NCI testing

The compounds were tested against a panel of 60 human cancer cell lines at the National Cancer Institute, Rockville, MD using the assay presented in ref.[26]

MTS assay on normal fibroblasts and MCF7 breast cancer cell line

Human gingival fibroblasts (HGF) or breast adenocarcinoma cells (MCF7, both from CLS Cell Lines Service GmbH, Eppelheim, Germany) were seeded into 96-well tissue culture-treated plates in α-MEM medium with 10% fetal bovine serum. The next day, cells were incubated with different concentrations (10^{-5}, 2.5×10^{-5}, 5×10^{-5}, 7.5×10^{-5} and 10^{-4} M) of compound **2**, quinoline, quinoxaline, **3g** and **3h** for 24h. CellTiter 96® AQueous One Solution Cell Proliferation Assay (Promega, Madison, WI USA) was used to determine cell viability, according to the manufacturer's instructions. A FLUOstar® Omega microplate reader (BMG LABTECH, Ortenberg, Germany) was used to record absorbance readings at 490 nm of triplicate experiments. Treated cells' viability was calculated as percentage of untreated cells' viability and data were represented as means ± standard deviations. Compound concentrations that induce 50% decrease in cell viability (IC_{50}) were determined for each cell line from the dose–response curves generated with GraphPad Prism 8 software.

CONCLUSIONS

In this manuscript, we successfully synthesized six novel monoquaternary salts and two physical arrangements that were unexpectedly generated during the synthesis process, starting from various N-heterocycles. All compounds were fully structurally characterized, including XRD in the case of mixture **3g**. Our primary objective was to compare their antitumor activities across a panel of 60 human cancer cell lines. Impressively, mixtures **3g** and **3h** exhibited remarkable inhibitory action against leukemia, melanoma, and colon cancer cell lines. Furthermore, in the case of MCF7 breast cancer cells, we can say that the optimal concentration of compound **2** would be $5x10^{-5}$ M, while for mixtures **3g** and **3h** effective antitumoral activity could be achieved with $2.5x10^{-5}$ M. These findings hold significant promise for potential therapeutic applications. The formation of supramolecular assemblies through hydrogen bonding in the physical mixtures allows for stronger interactions with the target biomolecules, leading to increased antitumor activity compared to the individual quinoline and quinoxaline compounds.

Acknowledgments. The authors acknowledge National Cancer Institute for the anticancer evaluation of the compounds on their 60-cell panel. The testing was performed by the Developmental Therapeutics Program, Division of Cancer Treatment and Diagnosis (the URL to the Program's website: http://dtp.cancer.gov/). We also thank to CERNESIM Research Center from "Alexandru Ioan Cuza" University of Iasi for recording the NMR experiments.

REFERENCES

1. W. Li, F. Xu, W. Shuai, H. Sun, H. Yao, C. Ma, S. Xu, H. Yao, Z. Zhu, D. H. Yang, Z. S. Chen and J. Xu, *J. Med. Chem.*, **2019**, *62*, 993–1013, doi:10.1021/acs.jmedchem.8b01755.
2. D. Diaconu, V. Antoci, V. Mangalagiu, D. Amariucai-Mantu and I. I. Mangalagiu, *Sci. Rep.*, **2022**, *12*, 1–17, doi:10.1038/s41598-022-21435-6.
3. L. Oniciuc, D. Amăriucăi-Mantu, D. Diaconu, V. Mangalagiu, R. Danac, V. Antoci and I. I. Mangalagiu, *Int. J. Mol. Sci.*, **2023**, *24*, doi:10.3390/ijms24098124.
4. F. Xu, M. Liu, Y. Liao, Y. Zhou, P. Zhang, Y. Zeng and Z. Liu, *Phytomedicine*, **2022**, *104*, 154314–154320, doi:10.1016/j.phymed.2022.154314.
5. Y. T. Han, J.-W. Jung and N.-J. Kim, *Curr. Org. Chem.*, **2017**, *21*, 1265–1291, doi:10.2174/1385727282166170221150901.
6. Z. Gu, Y. Li, S. Ma, S. Li, G. Zhou, S. Ding, J. Zhang, S. Wang and C. Zhou, *RSC Adv.*, **2017**, *7*, 41869–41879, doi:10.1039/c7ra08138c.
7. D. Mantu, D. Maftei, D. Iurea, C. Ursu and V. Bejan, *Med. Chem. Res.*, **2014**, *23*, 2909–2915, doi:10.1007/s00044-013-0878-8.
8. L. Popovici, R. M. Amarandi, I. I. Mangalagiu, V. Mangalagiu and R. Danac, *J. Enzyme Inhib. Med. Chem.*, **2019**, *34*, 230–243, doi:10.1080/14756366.2018.1550085.
9. T. S. da Silva, M. da Silva Souza, A. D. Andricopulo and F. Coelho, *RSC Adv.*, **2023**, *13*, 20264–20270, doi:10.1039/d3ra03395c.
10. A. Wójcicka and A. Redzicka, *Pharmaceuticals*, **2021**, *14*, doi:10.3390/ph14040354.
11. Y. Ling, Z. Y. Hao, D. Liang, C. L. Zhang, Y. F. Liu and Y. Wang, *Drug Des. Devel. Ther.*, **2021**, *15*, 4289–4338, doi:10.2147/DDDT.S329547.
12. D. Amariucai-Mantu, V. Antoci, M. C. Sardaru, C. M. Al Matarneh, I. Mangalagiu and R. Danac, *Phys. Sci. Rev.*, **2023**, *8*, 2583–2645. https://doi.org/10.1515/psr-2021-0030.
13. C. M. Al Matarneh, M. O. Apostu, I. I. Mangalagiu and R. Danac, *Tetrahedron*, **2016**, *72*, 4230–4238, doi:10.1016/j.tet.2016.05.061.
14. C. M. Al Matarneh, C. I.;Ciobanu, M. O. Apostu, I. I. Mangalagiu and R. Danac, *Comptes. Rendus. Chim.*, **2018**, *21*, doi:10.1016/j.crci.2017.11.003.

15. C. Al-Matarneh, I. Rosca, S. Shova and R. Danac, *J. Serbian Chem. Soc.*, **2021**, *86*, 901–915, doi:10.2298/jsc200819057a.
16. C. Al Matarneh, C. I. Ciobanu, V. Mangalagiu, G. Zbancioc and R. Danac, *Rev. Chim.* (Bucharest), **2020**, *71*, 287–293, doi:10.37358/RC.20.3.7999.
17. C. Maria, A. Matarneh, R. M. Amarandi, A. M.; Craciun, I. I. Mangalagiu, G. Zbancioc and R. Danac, *Molecules*, **2020**, *25*, 527–543. https://doi.org/10.3390/molecules25030527.
18. M. C. Al-Matarneh, R.-M. Amărandi, I. I. Mangalagiu and R. Danac, *Molecules*, **2021**, *26*, 2066, doi:10.3390/molecules26072066.
19. R.-M. Amărandi, M.-C. Al-Matarneh, L. Popovici, C. I. Ciobanu, A. Neamțu, I. I. Mangalagiu and R. Danac, *Pharmaceuticals*, **2023**, *16*, 865, doi:10.3390/ph16060865.
20. C. M. Al Matarneh, C. I. Ciobanu, I. I. Mangalagiu and R. Danac, *J. Serbian Chem. Soc.*, **2016**, *81*, doi:10.2298/JSC150514084A.
21. D. Mantu, E. Ene, V. Antocia and A. M. Zbanciocb, *Acta Chem. Iasi*, **2013**, *21*, 9–18, doi:10.2478/achi-2013-0002.
22. Rigaku Oxford Diffraction CrysAlis Pro Software System 2015.
23. G. M. Sheldrick, *Acta Crystallogr. Sect. A Found Crystallogr.*, **2015**, *71*, 3–8, doi:10.1107/S2053273314026370.
24. G. M. Sheldrick, *Acta Crystallogr. Sect. C Struct. Chem.*, **2015**, *71*, 3–8, doi:10.1107/S2053229614024218.
25. O. V. Dolomanov, L. J. Bourhis, R. J. Gildea, J. A. K. Howard and H. Puschmann, *J. Appl. Crystallogr.*, **2009**, *42*, 339–341, doi:10.1107/S0021889808042726.
26. R. H. Shoemaker, *Nat. Rev. Cancer*, **2006**, *6*, 13–23.